Wideband Aperture-Overlapped MIMO Antennas Naturally Integrating Mode Orthogonal and Parasitic Decoupling Schemes

Jiangwei Sui, *Member, IEEE*, Cuixia Huang, *Student Member, IEEE*, Junru Li, *Member, IEEE*, Xiangwei Zhu, *Member, IEEE*, and Du Li, *Member, IEEE*

***Abstract*—In this letter, a wideband self-decoupling scheme is proposed for multiple-input–multiple-output (MIMO) antennas. Based on the mode orthogonal decoupling scheme, when the proposed differential mode antenna is integrated with a loop branch, it will be decoupled at one frequency f_1. Moreover, the parasitic branch in the proposed antenna naturally works as a parasitic decoupling element, so it will achieve decoupling at a second frequency f_2 simultaneously. Two demonstrational examples working in the N79 band (4.4 GHz to 5 GHz) are studied. The results show that the MIMO antennas using the proposed scheme can achieve a wideband isolation greater than 26.4 dB across the whole band with two transmission zeros. Taking into consideration the attractive integration free from differential feeding structures and wideband high isolation, the proposed integrating decoupling scheme may provide a new vision for the MIMO antenna designs.**

***Index Terms*—Antenna decoupling, aperture-overlapped, dipole mode, mobile terminals, multiple-input–multiple-output (MIMO), mutual coupling, self-decoupled.**

I. Introduction

According to Shannon's theorem, to further improve the channel capacity of the wireless communication system, wider frequency bands can be utilized [1]. Besides, the multiple-input–multiple-output (MIMO) technique has been widely adopted to enhance spectrum efficiency. However, with the increase of antennas, the mutual coupling between the wideband MIMO antennas has become a thorny issue [2].

To deal with the antenna mutual coupling in mobile terminals, many efforts have been devoted, and these methods can be divided into two main categories. In the first categories, well-designed decoupling structures are introduced to obstruct or cancel out the original couplings, such as neutralization lines [3], [4], [5], [6], decoupling networks [7], [8], [9], [10], parasitic elements [11], [12], special ground structures [13], [14], [15], and decoupling capacitors [16], [17], [18]. However, the bulky size of the introduced structures usually conflicts with the requirement of antenna miniaturization in mobile terminals [19].

Another category is the self-decoupling scheme. First, the two antennas can be self-decoupled by arranging their geometries delicately [20], [21], [22]. Besides, the decomposed common mode and differential mode of the antenna system can also be adjusted to cancel with each other [23], [24], [25], [26]. Moreover, two antennas can be self-decoupled using orthogonal features, such as orthogonal modes [27], [28], [29], [30], [31], [32], [33], [34], orthogonal polarizations [35], [36], [37], and orthogonal patterns [38], among which some can support wideband applications [31], [33]. However, these wideband designs all require differential-feeding structures, which usually suffer from the integration challenge of antenna and printed circuit board (PCB) in mobile terminals. Recently, a self-multipath concept has been proposed for wideband MIMO antennas [39]. Nevertheless, a complex matching circuit is required for each antenna to trade off the bandwidth.

In this letter, a novel wideband decoupling scheme is proposed by naturally integrating the mode orthogonal and parasitic decoupling schemes. Compared with the existing wideband decoupling methods, especially the orthogonality-based decoupling techniques, the proposed method has two distinct advantages.

1) The proposed scheme naturally integrates mode orthogonal decoupling and parasitic decoupling for the aperture-overlapped structures, so two transmission zeros are inherently generated to achieve a compact self-decoupling.
2) The proposed differential mode antenna is fed using the coupled microstrip line but not the coaxial cable or a Balun chip to excite the in-phase current mode, so it is more attractive for integration of the antenna body and PCB in mobile terminals.

II. Decoupling Mechanism

A. Schematic Diagram

Fig. 1(a) presents the traditional mode orthogonal decoupling scheme [29], where a dipole is adopted as the differential mode antenna, and the loop antenna is selected for the common mode one. For the dipole antenna, if the antenna is divided equally into two parts, the current of these two parts will be the same, which is denoted as I_1. On the contrary, for the loop antenna, the currents on the left part and the right part are of opposite directions, which can be denoted as I_2 and $-I_2$, presenting a typical common mode.

Manuscript received 9 April 2024; accepted 20 April 2024. Date of publication 30 April 2024; date of current version 6 August 2024. This work was supported in part by the National Key R&D Program of China under Grant 2021YFA0716500; in part by the National Natural Science Foundation of China under Grant 62201625; and in part by the Guangdong Basic and Applied Basic Research Foundation under Grant 2021A1515110728. *(Corresponding author: Du Li.)*

The authors are with the School of Electronics and Communication Engineering and Shenzhen Key Laboratory of Navigation and Communication Integration, Shenzhen Campus of Sun Yat-sen University, Shenzhen 518000, China (e-mail: suijw@mail.sysu.edu.cn; huangcx7@mail2.sysu.edu.cn; lijr85@mail.sysu.edu.cn; zhuxw666@mail.sysu.edu.cn; lidu5@mail.sysu.edu.cn).

Digital Object Identifier 10.1109/LAWP.2024.3395270

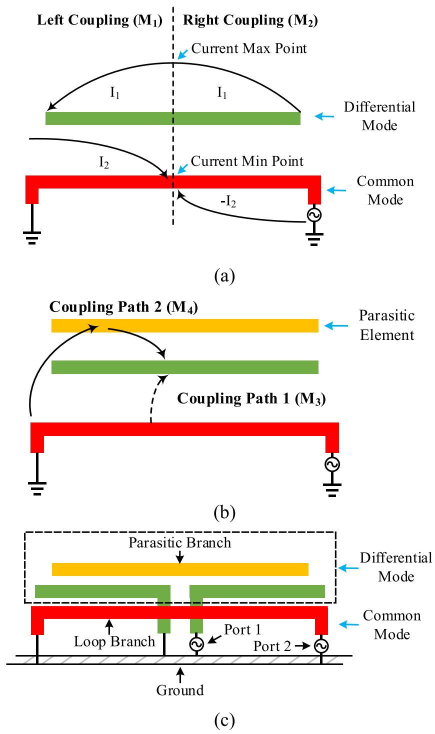

Fig. 1. Decoupling mechanism of the proposed wideband MIMO antennas. (a) Traditional mode orthogonal decoupling scheme. (b) Traditional parasitic decoupling scheme. (c) Proposed wideband decoupling scheme.

When the two antennas are integrated, the total coupling can be obtained by the superposition of the left part and the right part, M_1 and M_2. It is well known the radiation field is linearly dependent on the current distribution of the antenna body, so the coupling M_1 and M_2 can be roughly described as follows:

$$M_1 = C_0 f(I_1) \times f(I_2) \quad \text{(1a)}$$

$$M_2 = C_0 f(I_1) \times [-f(I_2)] \quad \text{(1b)}$$

where the f represents the transform function between the current and the corresponding field, and C_0 is the related transformation coefficient. Therefore, the total coupling can be readily achieved

$$M_{total} = M_1 + M_2 = 0 \quad (2)$$

which means that the decoupling is obtained at one certain frequency f_1.

Besides, the parasitic concept is another effective decoupling scheme, as is shown in Fig. 1(b). Without loss of generality, here, the above-studied dipole antenna and the loop antenna are still used for convenience. At another frequency f_2, these two antennas are strongly coupled through the coupling path 1 if no decoupling scheme is imposed, as the coupling M_3 denotes in Fig. 1(b). To mitigate this coupling, a parasitic element is introduced, so that the coupling path 2 will be generated to bring another coupling M_4. By properly selecting the parasitic element and adjusting the antenna geometry, the total coupling can also diminish

$$M_{total} = M_3 + M_4 = 0. \quad (3)$$

To enlarge the decoupling bandwidth, a decoupling method by naturally integrating these two schemes is proposed. As is depicted in Fig. 1(c), the loop branch is still used as the common mode antenna, while the differential mode antenna is a new antenna type. The parasitic branch in the proposed antenna works as a parasitic decoupling element at f_2, and due to the boundary condition of two open ends for the parasitic branch, it does not affect the differential mode f_1.

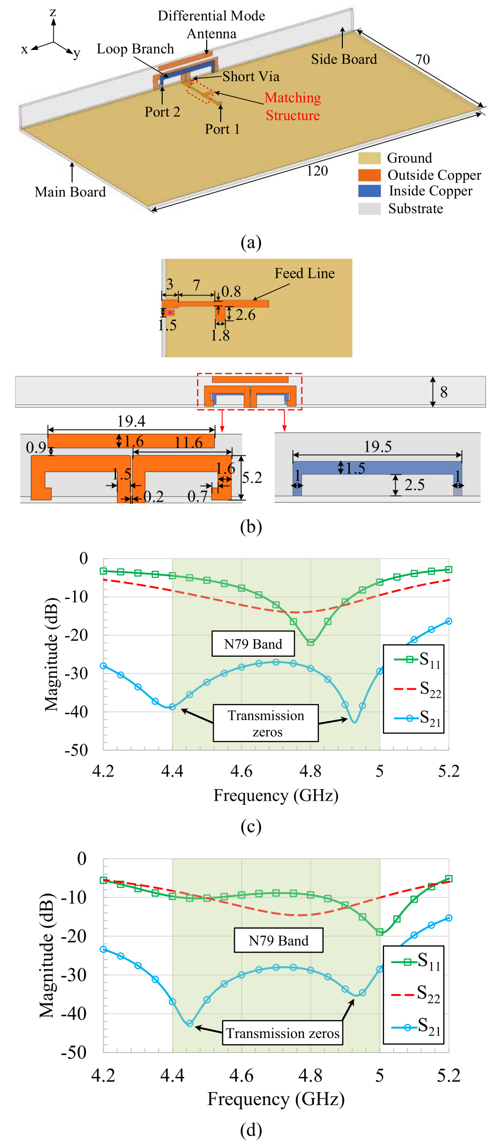

Fig. 2. Geometries and simulated S-parameters of proposed vertically-placed antenna pair. (a) Perspective view. (b) Detailed dimensions of the antenna element. The unit used here is mm. (c) S-parameters without matching structure at port 1. (d) S-parameters with matching structure at port 1.

A demonstrational example shown in Fig. 2 is further studied. The size of the main board is 120 mm × 70 mm, and the proposed antennas are vertically placed on a sideboard. In the simulation, the substrate is the FR4 with a relative permittivity of 4.4, loss tangent of 0.02, and thickness of 0.8 mm. The simulated S-parameters without the matching structure at port 1 are presented in Fig. 2(c), showing a wideband isolation with two transmission zeros at 4.45 GHz and 4.9 GHz. It is observed that without the matching structure, there is only one resonance for S_{11}, and the impedance matching cannot cover the whole band from 4.4 GHz to 5 GHz. To enhance the S_{11}, a matching structure consisting of a cascaded microstrip line and a short

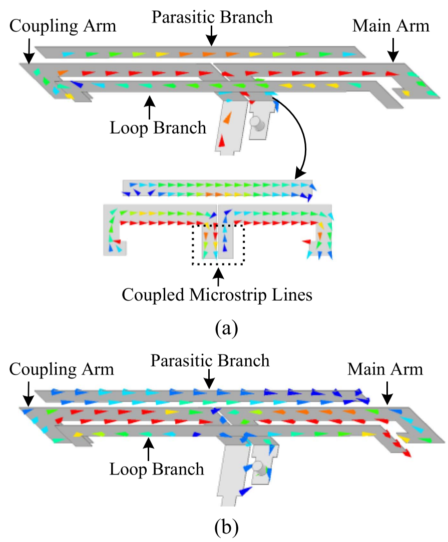

Fig. 3. Current distribution of the proposed wideband MIMO antennas at 4.45 GHz. (a) Port 1 excited. (b) Port 2 excited.

stub, as shown in Fig. 2(a), is designed for port 1. It is seen from Fig. 2(d) that another resonance for S_{11} is introduced after using the matching structure, achieving an impedance matching better than -9 dB across the desired band.

B. Decoupling Mechanism of the First Transmission Zero

It is well-known that for a dipole antenna, a differential feeding structure is usually required to excite the in-phase current mode, for example, the coaxial cable in [30] and the balun chip in [31]. However, the balun chip will introduce undesired design complexity and cost, and the coaxial cable cannot be directly integrated with the PCB in mobile terminals. In the proposed differential mode antenna, the vertical portions of the main arm and the coupling arm form a section of coupled transmission lines, whose currents are opposite to each other, as illustrated in Fig. 3(a). Therefore, due to the current continuity, the currents on the horizontal portions of the main arm and coupling arm are in the same directions, and the currents on the parasitic branch are also in phase due to the open-end boundary condition when port 1 is excited at 4.45 GHz, presenting a typical differential mode.

Differently, when port 2 is excited, as illustrated in Fig. 3(b), the current directions on the two arms are opposite, presenting a common mode. Therefore, the decoupling mechanism of the first transmission zero at 4.45 GHz lies in the orthogonal characteristics of the corresponding two modes.

C. Decoupling Mechanism of the Second Transmission Zero

The *S*-parameters with and without the parasitic branch are compared in Fig. 4. It is seen that the second transmission zero at 4.9 GHz disappears when the parasitic branch is taken away. It is further demonstrated in Fig. 5 that the second transmission zero will be effectively adjusted by tuning the length of the parasitic branch, l_1, with about 100 MHz decrease to 0.4 mm increase of l_1. Therefore, it can be concluded that the second transmission zero can be independently controlled by tuning the length of the parasitic branch.

A design guideline can be summarized as follows.

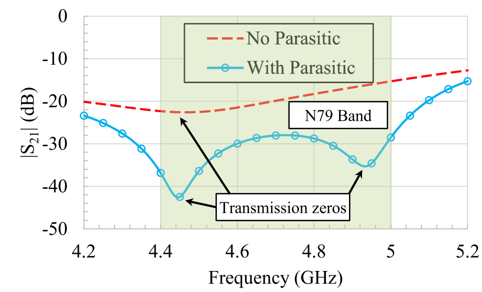

Fig. 4. *S*-parameters without and with the parasitic branch.

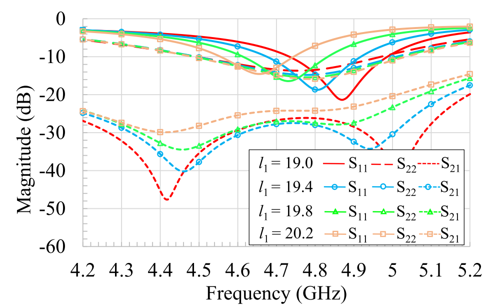

Fig. 5. Parametric study of the length of the parasitic branch.

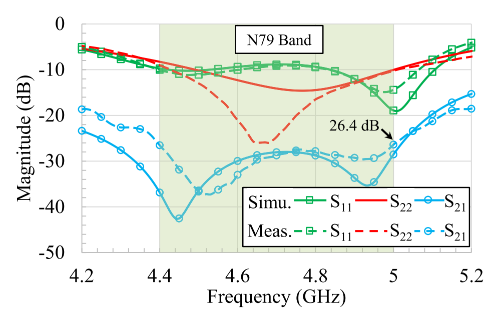

Fig. 6. Comparison of simulated and measured *S*-parameters of the proposed vertically-placed wideband MIMO antennas.

1) First, the length of the two arms and the loop branch is first selected to locate the first transmission zero at f_1.
2) Then, the length of the parasitic branch is adjusted to locate the second transmission zero at f_2. The branch length is approximately $\lambda/2$ at f_2, as a dipole-type parasitic element.
3) Finally, the other dimensions, for example, the vertical portion can be utilized to fine-tune the matching impedance.

III. Results and Discussions

A. Vertically-Placed Wideband MIMO Antennas

The above-studied vertically-placed MIMO antennas are fabricated and measured. As expected in Fig. 6, there are two transmission zeros within the N79 band from 4.4 GHz to 5 GHz, and the isolation is better than 26.4 dB across the whole band. As the results show in Fig. 7, the average efficiency for port 1 is about 66% and about 79% for port 2, demonstrating a good performance. Besides, the envelope correlation coefficients (ECCs) are always lower than 0.003 across the whole N79 band, showing a good performance for spatial multiplexing.

TABLE I
COMPARISON OF SOME RECENTLY PROPOSED ORTHOGONALITY-BASED MIMO ANTENNAS

Ref.	**Decoupling Mechanism**	**Transmission Zero Number**	**Feeding of D-Mode**	**Frequency Band (GHz)**	**Antenna Size (λ_0^2)***	**Antenna Height (mm)**	**Isolation**	**Total Efficiencies**
[29][2018]	Mode orthogonal	1	Coupled feeding	3.4 – 3.6	0.14×0.081	7	> 20 dB	61.6 – 72.9 % 49 – 56.4 %
[31][2020]	Mode orthogonal	2	Balun	3.3 – 5	0.553 × 0.1	7.5	> 21 dB	58.9 – 88.6 % 31.6 – 76.7 %
[36][2019]	Polarization orthogonal	1	Coaxial cable	3.4 – 3.6	0.291×0.081	7	> 23.9 dB	56.2 – 64.7 % 35.2 – 49.3 %
[38][2020]	Pattern orthogonal	1	Coaxial cable	2.4 – 2.5	0.49 × 0.21	18.5	> 25 dB	77 – 85 %
Proposed	Mode orthogonal + Parasitic decoupling	2	Microstrip line	4.4 – 5	0.376 × 0.125	8	> 26.4 dB	69.2 – 86.2 % 56.8 – 72.9 %

* Here , λ_0 denotes the wavelength in free space at the center frequency of the band.

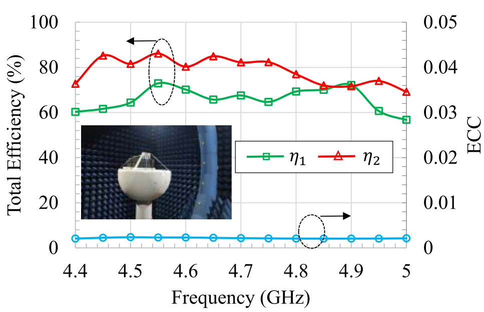

Fig. 7. Measured total efficiencies and ECCs of the proposed vertically-placed wideband MIMO antennas.

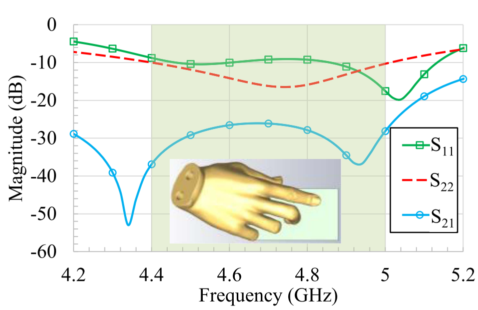

Fig. 8. *S*-parameters with hand's effect.

For the typical single-hand type effect shown in Fig. 8, it is found that the S_{11} and S_{22} almost keep the same as those without the hand model, similar to the results shown in [6], and the two transmission zeros also maintain so that high isolation better than 26 dB is still achieved in the whole N79 band, showing a robust decoupling for the user's effect.

It is seen from Table I that all the prior designs except that in [31] can only generate one transmission zero, so the achieved decoupling bandwidth is somewhat not too wide. Although the design in [31] can support wideband decoupling, it cannot support the aperture-shared applications, so the size is larger than the proposed work. Moreover, a balun chip is required in [31] to generate the differential mode antenna, which sacrifices the eventual total efficiencies. Furthermore, the achieved isolation is higher than all the prior designs.

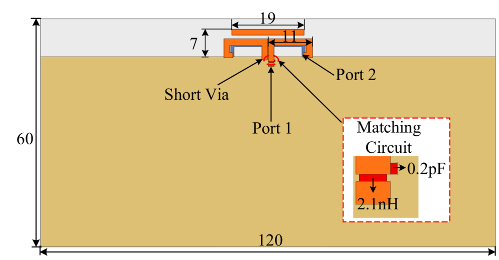

Fig. 9. Geometries of the proposed planar wideband MIMO antennas.

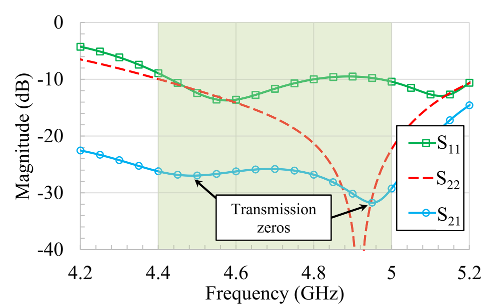

Fig. 10. Simulated *S*-parameters of the planar wideband MIMO antennas.

B. Planar-Placed Wideband MIMO Antennas

A second example of planar configuration is justified in this part, as shown in Fig. 9. A typical L-typed LC circuit consisting of a series 2.1 nH inductor and a parallel 0.2 pF capacitor is utilized to match the impedance of port 1, showing a good capability of miniaturization. The simulated *S*-parameters are presented in Fig. 10. As expected, there are two transmission zeros with isolation better than 26 dB throughout the whole N79 band, justifying the generality of the proposed scheme.

IV. CONCLUSION

In this letter, a wideband self-decoupling scheme is proposed by naturally integrating two decoupling methods. Benefiting from the special configuration of the proposed differential mode antenna, when it is integrated with a loop antenna, there will exist the mode orthogonal and parasitic decoupling simultaneously, so two transmission zeros can be generated to achieve a wide-band decoupling. Two demonstrational examples are designed to justify the proposed scheme.

REFERENCES

[1] WRC-15 Press Release, Nov. 27, 2015, World radiocommunication conference allocates spectrum for future innovation, [Online]. Available: http://www.itu.int/net/pressoffice/press_releases/2015/56.aspx

[2] X. Chen, S. Zhang, and Q. Li, "A review of mutual coupling in MIMO systems," *IEEE Access*, vol. 6, pp. 24706–24719, 2018.

[3] A. Diallo, C. Luxey, P. Le Thuc, R. Staraj, and G. Kossiavas, "Study and reduction of the mutual coupling between two mobile phone PIFAs operating in the DCS1800 and UMTS bands," *IEEE Trans. Antennas Propag.*, vol. 54, no. 11, pp. 3063–3074, Nov. 2006.

[4] Y. Wang and Z. Du, "A wideband printed dual-antenna with three neutralization lines for mobile terminals," *IEEE Trans. Antennas Propag.*, vol. 62, no. 3, pp. 1495–1500, Mar. 2014.

[5] C. D. Xue, X. Y. Zhang, Y. F. Cao, Z. Hou, and C. F. Ding, "MIMO antenna using hybrid electric and magnetic coupling for isolation enhancement," *IEEE Trans. Antennas Propag.*, vol. 65, no. 10, pp. 5162–5170, Oct. 2017.

[6] L. Sun, Y. Li, and Z. Zhang, "Wideband integrated quad-element MIMO antennas based on complementary antenna pairs for 5G smartphones," *IEEE Trans. Antennas Propag.*, vol. 69, no. 8, pp. 4466–4474, Aug. 2021.

[7] S. C. Chen, Y. S. Wang, and S. J. Chung, "A decoupling technique for increasing the port isolation between two strongly coupled antennas," *IEEE Trans. Antennas Propag.*, vol. 56, no. 12, pp. 3650–3658, Dec. 2008.

[8] J. Sui and K. L. Wu, "A general T-stub circuit for decoupling of two dual-band antennas," *IEEE Trans. Microw. Theory Techn.*, vol. 65, no. 6, pp. 2111–2121, Jun. 2017.

[9] M. Li, Y. Zhang, D. Wu, K. L. Yeung, L. Jiang, and R. Murch, "Decoupling and matching network for dual-band MIMO antennas," *IEEE Trans. Antennas Propag.*, vol. 70, no. 3, pp. 1764–1775, Mar. 2022.

[10] Y. F. Cheng and K. K. M. Cheng, "Compact wideband decoupling and matching network design for dual-antenna array," *IEEE Antennas Wireless Propag. Lett.*, vol. 19, no. 5, pp. 791–795, May 2020.

[11] B. K. Lau and J. B. Andersen, "Simple and efficient decoupling of compact arrays with parasitic scatterers," *IEEE Trans. Antennas Propag.*, vol. 60, no. 2, pp. 464–472, Feb. 2012.

[12] H. Xu, H. Zhou, S. Gao, H. Wang, and Y. Cheng, "Multimode decoupling technique with independent tuning characteristic for mobile terminals," *IEEE Trans. Antennas Propag.*, vol. 65, no. 12, pp. 6739–6751, Dec. 2017.

[13] C. Y. Chiu, C. H. Cheng, R. D. Murch, and C. R. Rowell, "Reduction of mutual coupling between closely-packed antenna element," *IEEE Trans. Antennas Propag.*, vol. 55, no. 6, pp. 1732–1738, Jun. 2007.

[14] J. F. Li, Q. X. Chu, and T. G. Huang, "A compact wideband MIMO antenna with two novel bent slits," *IEEE Trans. Antennas Propag.*, vol. 60, no. 2, pp. 482–489, Feb. 2012.

[15] S. Zhang, B. K. Lau, Y. Tan, Z. Ying, and S. He, "Mutual coupling reduction of two PIFAs with a T-shape slot impedance transformer for MIMO mobile terminal," *IEEE Trans. Antennas Propag.*, vol. 60, no. 3, pp. 1521–1531, Mar. 2012.

[16] C. Deng, D. Liu, and X. Lv, "Tightly arranged four-element MIMO antennas for 5G mobile terminals," *IEEE Trans. Antennas Propag.*, vol. 67, no. 10, pp. 6353–6361, Oct. 2019.

[17] J. Sui, Y. Dou, X. Mei, and K. L. Wu, "Self-curing decoupling technique for MIMO antenna arrays in mobile terminals," *IEEE Trans. Antennas Propag.*, vol. 68, no. 2, pp. 838–849, Feb. 2020.

[18] J. Sui, C. Huang, and Y. F. Cheng, "Multi-element fully-decoupled inverted-F antennas for mobile terminals," *IEEE Trans. Antennas Propag.*, vol. 70, no. 11, pp. 10076–10085, Nov. 2022.

[19] H. Chen and A. Zhao, "LTE antenna design for mobile phone with metal frame," *IEEE Antennas Wireless Propag. Lett.*, vol. 15, pp. 1462–1465, 2016.

[20] K. L. Wong, C. Y. Tsai, and J. Y. Lu, "Two asymmetrically mirrored gap-coupled loop antennas as a compact building block for eight-antenna MIMO array in the future smartphone," *IEEE Trans. Antennas Propag.*, vol. 65, no. 4, pp. 1765–1778, Apr. 2017.

[21] Z. Ren, A. Zhao, and S. Wu, "MIMO antenna with compact decoupled antenna pairs for 5G mobile terminals," *IEEE Antennas Wireless Propag. Lett.*, vol. 18, no. 7, pp. 1367–1371, Jul. 2019.

[22] J. Sui and K. L. Wu, "A self-decoupled antenna array using inductive and capacitive couplings cancellation," *IEEE Trans. Antennas Propag.*, vol. 68, no. 7, pp. 5289–5296, Jul. 2020.

[23] L. Sun, Y. Li, Z. Zhang, and H. Wang, "Self-decoupled MIMO antenna pair with shared radiator for 5G smartphones," *IEEE Trans. Antennas Propag.*, vol. 68, no. 5, pp. 3423–3432, May 2020.

[24] B. Yang, Y. Xu, J. Tong, Y. Zhang, Y. Feng, and Y. Hu, "Tri-port antenna with shared radiator and self-decoupling characteristic for 5G smartphone application," *IEEE Trans. Antennas Propag.*, vol. 70, no. 6, pp. 4836–4841, Jun. 2022.

[25] A. Zhang, K. Wei, Y. Hu, and Q. Guan, "High-isolated coupling-grounded patch antenna pair with shared radiator for the application of 5G mobile terminals," *IEEE Trans. Antennas Propag.*, vol. 70, no. 9, pp. 7896–7904, Sep. 2022.

[26] L. Sun, Y. Li, Z. Zhang, and H. Wang, "Antenna decoupling by common and differential modes cancellation," *IEEE Trans. Antennas Propag.*, vol. 69, no. 2, pp. 672–682, Feb. 2021.

[27] H. Li, Z. T. Miers, and B. K. Lau, "Design of orthogonal MIMO handset antennas based on characteristic mode manipulation at frequency bands below 1 GHz," *IEEE Trans. Antennas Propag.*, vol. 62, no. 5, pp. 2756–2766, May 2014.

[28] X. Zhao, S. P. Yeo, and L. C. Ong, "Decoupling of inverted-F antennas with high-order modes of ground plane for 5G mobile MIMO platform," *IEEE Trans. Antennas Propag.*, vol. 66, no. 9, pp. 4485–4495, Sep. 2018.

[29] L. Sun, H. Feng, Y. Li, and Z. Zhang, "Compact 5G MIMO mobile phone antennas with tightly arranged orthogonal-mode pairs," *IEEE Trans. Antennas Propag.*, vol. 66, no. 11, pp. 6364–6369, Nov. 2018.

[30] H. Xu, S. S. Gao, H. Zhou, H. Wang, and Y. Cheng, "A highly integrated MIMO antenna unit: Differential/common mode design," *IEEE Trans. Antennas Propag.*, vol. 67, no. 11, pp. 6724–6734, Nov. 2019.

[31] L. Sun, Y. Li, Z. Zhang, and Z. Feng, "Wideband 5G MIMO antenna with integrated orthogonal-mode dual-antenna pairs for metal-rimmed smartphones," *IEEE Trans. Antennas Propag.*, vol. 68, no. 4, pp. 2494–2503, Apr. 2020.

[32] A. Ren, Y. Liu, and C. Y. D. Sim, "A compact building block with two shared-aperture antennas for eight-antenna MIMO array in metal-rimmed smartphone," *IEEE Trans. Antennas Propag.*, vol. 67, no. 10, pp. 6430–6438, Oct. 2019.

[33] W. F. Zeng, F. C. Chen, and Q. X. Chu, "Bandwidth-enhanced 5G mobile phone antenna pair with tunable electric field null," *IEEE Trans. Antennas Propag.*, vol. 71, no. 2, pp. 1960–1964, Feb. 2023.

[34] W. Hu et al., "Dual-band antenna pair with high isolation using multiple orthogonal modes for 5G smartphones," *IEEE Trans. Antennas Propag.*, vol. 71, no. 2, pp. 1949–1954, Feb. 2023.

[35] M. Y. Li et al., "Eight-port orthogonally dual-polarized antenna array for 5G smartphone applications," *IEEE Trans. Antennas Propag.*, vol. 64, no. 9, pp. 3820–3830, Sep. 2016.

[36] L. Chang, Y. Yu, K. Wei, and H. Wang, "Polarization-orthogonal co-frequency dual antenna pair suitable for 5G MIMO smartphone with metallic bezels," *IEEE Trans. Antennas Propag.*, vol. 67, no. 8, pp. 5212–5220, Aug. 2019.

[37] L. Chang, Y. Yu, K. Wei, and H. Wang, "Orthogonally polarized dual antenna pair with high isolation and balanced high performance for 5G MIMO smartphone," *IEEE Trans. Antennas Propag.*, vol. 68, no. 5, pp. 3487–3495, May 2020.

[38] Y. F. Cheng and K. K. M. Cheng, "Decoupling of two-element printed-dipole antenna array by optimal meandering design," *IEEE Trans. Antennas Propag.*, vol. 68, no. 11, pp. 7328–7338, Nov. 2020.

[39] A. Zhang, K. Wei, and Z. Zhang, "Multiband and wideband self-multipath decoupled antenna pairs," *IEEE Trans. Antennas Propag.*, vol. 71, no. 7, pp. 5605–5615, Jul. 2023.